Article

# Falloff Curves of the Reaction CF$_3$ (+M) → CF$_2$ + F (+M)

C. J. Cobos, G. Knight, L. Sölter, E. Tellbach, and J. Troe*

Cite This: *J. Phys. Chem. A* 2020, 124, 1235−1239

Read Online

ACCESS | 📊 Metrics & More | 📰 Article Recommendations | 🆂🅸 Supporting Information

ABSTRACT: The thermal dissociation reaction CF$_3$ (+Ar) → CF$_2$ + F (+Ar) was studied in incident and reflected shock waves by monitoring UV absorption signals of the primary dissociation product CF$_2$. CF$_3$ radicals were produced by thermal decomposition of CF$_3$I. Accounting for secondary reactions of F atoms, rate constants for the unimolecular dissociation were derived. Experimental parts of the falloff curves were obtained over the ranges 1544−2106 K and $1.0 \times 10^{-5} \leq$ [Ar] $\leq 9.3 \times 10^{-5}$ mol cm^{-3}. Theoretical modeling allowed for a construction of the full falloff curves connecting the limiting low-pressure rate constants k_0 = [Ar] 2.5×10^{18} $(T/2000$ K$)^{-5.1}$ exp $(-42\,450$ K$/T)$ cm^3 mol^{-1} s^{-1} with the limiting high-pressure rate constants k_∞ = 1.6×10^{16} $(T/2000$ K$)^{-1.3}$ exp $(-43\,250$ K$/T)$ s^{-1} (center broadening factors of F_{cent} = 0.25, 0.22, and 0.20 at 1500, 2000, and 2500 K, respectively, were used). The influence of simplifications of falloff expressions and of limiting rate constants on the representation of experimental data is discussed.
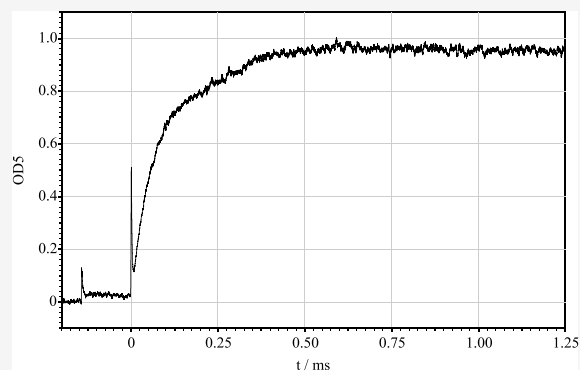
I. INTRODUCTION

The thermal dissociation reaction

$$CF_3(+Ar) \rightarrow CF_2 + F(+Ar) \tag{1}$$
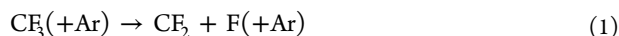
under typical shock wave conditions offers the opportunity to investigate unimolecular reaction behavior close to the low-pressure limit. The reaction has found some interest[1−3] because it plays a role in flame retardation by halons as well as in the high-temperature oxidation of fluorinated materials. In a first investigation,[1] it was assumed to be in the low-pressure limit. However, deviations from this behavior have been taken into consideration in later studies.[2,3] These were based on theoretical modeling of the limiting high-pressure rate constants k_∞ and estimates of the limiting low-pressure rate constants k_0, the latter employing adjusted average energies transferred per collision $\langle \Delta E \rangle$. This practice is quite common, when direct measurements of $\langle \Delta E \rangle$ are not available. One of the rare exceptions to this practice is the precursor of reaction 1, i.e., the dissociation of CF$_3$I,[4]

$$CF_3I(+Ar) \rightarrow CF_3 + I(+ Ar) \tag{2}$$
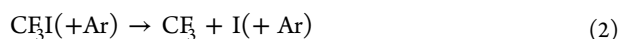
for which $\langle \Delta E \rangle$ has been determined in separate IR multiphoton excitation experiments (see work cited in ref 4). This reaction is also used in the present work. As measurements of k_0 continue to provide an important method to access $\langle \Delta E \rangle$, it appears of interest to inspect the accuracy of the approach. This not only concerns the analysis of k_0 but also the difference between modeled and measured rate constants k in the falloff range of the reaction. This is the focus of the present article.

A systematic modeling of falloff curves of unimolecular bond breaking and the reverse radical recombination reactions showed[5,6] that limiting low- and high-pressure rate constants are approached in different ways. Expressed in terms of broadening factors $F(x)$, defined by $k/k_\infty = [x/(1+x)]F(x)$ with $x = k_0/k_\infty$, this means that $F(x) \neq F(1/x)$. In a first systematic analysis of $F(x)$,[7] "symmetric broadening factors" (i.e., $F(x) = F(1/x)$) were assumed and approximated in the form

$$F(x) \approx F_{cent}^{1/[1+(\log x/N)^2]} \tag{3}$$

with "center broadening factors" F_{cent} and "widths" N given by $N \approx 0.75 - 1.27 \log F_{cent}$. The more detailed, master-equation based, study of refs 5, 6 led to asymmetric broadening factors (i.e., $F(x) \neq F(1/x)$) of the form

$$F(x) \approx (1 + x/x_0)/[1 + (x/x_0)^n]^{1/n} \tag{4}$$

with

$$n = [\ln 2/\ln(2/F_{cent})][1 - b + b(x/x_0)^q] \tag{5}$$

where $q = (F_{cent} - 1)/\ln(F_{cent}/10)$, x_0 in the range of 0.9−1.1 (mostly $x_0 \approx 1$), and b in the range 0.1−0.25 (mostly $b \approx 0.2$). Obviously, the F_{cent} in eqs 3−5 dominate the broadening of the falloff curves in comparison to the Lindemann−Hinshelwood

model (F_{cent} = 1) but the detailed form of $F(x)$ is of importance as well. The following study compares the approach of the falloff curves of reaction 1 to the low-pressure limit, considering eqs 3−5 as well as a master-equation solution described in ref 2. The present analysis is also accompanied by new experimental work.

In connection with the interest in extrapolations of falloff curves to limiting rate constants, the earlier decomposition studies of CF_3 decomposition were extended. The use of the decomposition of C_2F_6 or CF_3I as CF_3 precursors under the applied conditions led to contributions from secondary reactions. Since the work of refs 2, 3, more information on secondary reactions has been collected[4] such that their influence can be established with more certainty. Furthermore, theoretical modeling of the limiting rate constants has been advanced and applied to reaction 1. The earlier modeling from refs 2, 3 thus can also be extended.

II. EXPERIMENTAL TECHNIQUE AND RESULTS

The present measurements were carried out in a shock tube using both reflected and incident shock waves and the technique is described in detail in an earlier work (see, e.g., refs 3, 4, 8, 9). Like the previous studies,[1−3] the precursor for CF_3 was CF_3I, dissociating by reaction 2. As the UV absorption of CF_3 near 200 nm is too weak to allow for sufficiently sensitive detection of CF_3,[10] the broad UV continuum absorption of CF_2 was used to follow the dissociation. Absorption signals were recorded in the standard way, using a high-pressure Xe arc lamp (Osram XBO 150 W/4) as the light source, a quartz prism monochromator (Zeiss MQ3), photomultiplier, and an electronic data acquisition system. Compared to the earlier work of ref 8, more accurate absorption coefficients of CF_2 are now available, which allows for a more quantitative analysis of CF_2 yields recorded in the reaction. Reaction mixtures between 100 and 1000 ppm of CF_3I in Ar were employed and used as described in ref 4. CF_2 absorption−time profiles were followed at wavelengths in the range 230−270 nm, mostly at 248 nm, i.e., at the maximum of the broad absorption continuum. Typical signals are shown in Figures 1 and 2. The shown absorption signals OD5 correspond to the product OD5 = εx [CF_2], where x = 9.4
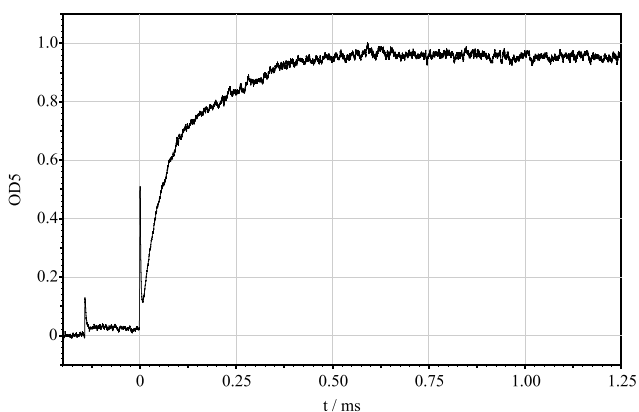

Figure 1. Absorption−time profile of CF_2 at 248 nm in the thermal decomposition of CF_3 behind a reflected shock wave (precursor 1054 ppm of CF_3I in Ar, incident shock wave: T = 977 K, [Ar] = $3.3 \cdot 10^{-5}$ mol cm^{-3}; reflected shock wave: T = 1874 K, [Ar] = $7.1 \cdot 10^{-5}$ mol cm^{-3}; OD5 = εx [CF_2] with x = 9.4 cm and ε = $2.7 \cdot 10^6$ cm^2 mol^{-1}; ε defined by the Lambert−Beer law in the form $I = I_0 \exp(-OD5)$).
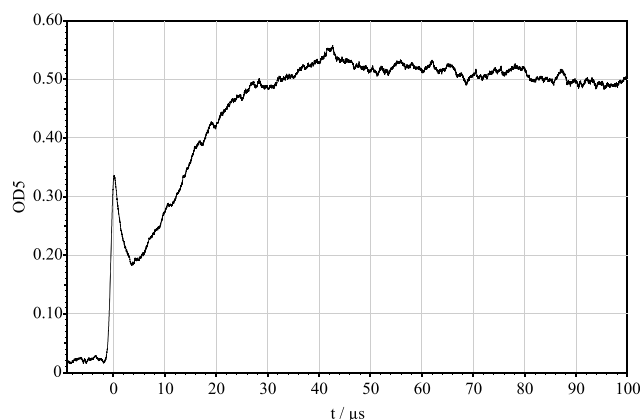

Figure 2. As Figure 1, but at T = 2049 K and [Ar] = $6.6 \cdot 10^{-5}$ mol cm^{-3} behind the reflected shock (527 ppm of CF_3I in Ar, ε = $2.3 \cdot 10^6$ cm^2 mol^{-1}).

cm and ε is the absorption coefficient of the Lambert−Beer law in the form $I = I_0 \exp(-OD5)$. The absorption behind the incident wave in Figure 1 is due to the precursor CF_3I. At the temperature of the incident wave (977 K), the decomposition of CF_3I just becomes noticeable. At the temperature of the reflected wave (1874 K), CF_3I almost instantaneously dissociates and only the formation of CF_2 is recorded. In Figure 2, the formation of CF_2 behind the reflected wave at 2048 K is rapid and just becomes separable from the Schlieren peak of the shock front. After CF_3 dissociation, CF_2 is essentially stable for the observation time of about 1.3 ms in Figure 1. In Figure 2, CF_2 dissociation starts to become noticeable, like those investigated in more detail in ref 3.

The approach to the final level of CF_2 could always be represented in the form

$$[CF_2] = [CF_2]_{t=\infty}\{1 - \exp(-kt)\} \qquad (6)$$

The final CF_2 concentration, $[CF_2]_{t=\infty}$, over the full range of precursor concentrations $[CF_3I]_{t=0}$ (100−1000 ppm of CF_3I in Ar) near 1900 K was found to be mostly of the order of 1/2 $[CF_3I]_{t=0}$ but increased to values near $[CF_3I]_{t=0}$ when the temperature was increased to values above 2000 K. This observation indicates that not only the unimolecular dissociation 1 was taking place but that secondary reactions like

$$F + CF_3(+Ar) \rightarrow CF_4(+Ar) \qquad (7)$$
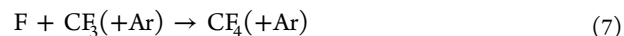
partly removed CF_3 by conversion into the thermally more stable CF_4, which does not absorb noticeably over the employed wavelength range. In addition to reaction 7, speculation about other secondary reactions was made in ref 3 but a quantitative analysis was difficult in that work. The work of ref 2, employing the dissociation of CF_3I in the presence of H_2O, focused on contributions of OH, O, and H to the $CF_3/CF_2/F$ system but, for the higher temperatures applied, could neglect reaction 7 and other reactions of the pure CF_3 system. Besides reaction 7, the present analysis of the CF_3 dissociation shows that the reverse of reaction 1

$$F + CF_2(+Ar) \rightarrow CF_3(+Ar) \qquad (8)$$
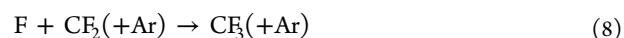
has to be taken into account. A possible influence of iodine atoms in the chain

$$I + CF_3 \rightarrow IF + CF_2 \qquad (9)$$

$$IF(+Ar) \rightarrow I + F(+Ar) \qquad (10)$$
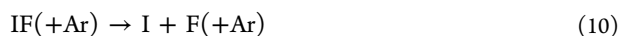
considered in ref 4 is also inspected. Reaction 8 would reduce the final CF_2 yield, $Y(CF_2) = [CF_2]_{t=\infty}/[CF_3]_{t=0}$, to values below 1/2 as long as steady state of F atoms is established in the sequence of reactions 1 and 7. On the other hand, the CF_2 yield would increase when reactions 9 and 10 are important. Besides the effective rate constant k in eq 6, the CF_2 yield $Y(CF_2)$, therefore, was of interest. The rate constants k_1 were derived from k and $Y(CF_2)$ by fitting the modeled $[CF_2]$ profiles to the experimental observations; see the following details.

While temperatures between 1803 and 2204 K were applied in ref 2, the present work extended the temperature range to 1544−2106 K. Furthermore, the range of bath gas concentrations $2.06 \times 10^{-6} < [Kr] < 5.71 \times 10^{-6}$ mol cm^{-3} from ref 2 in the present work was extended to $1.04 \cdot 10^{-5} < [Ar] < 9.28 \times 10^{-5}$ mol cm^{-3}. Consequently, deviation from the limiting low-pressure behavior became visible more clearly in the present work. The difference between the rate constant k_1 for reaction 1 and the measured k in eq 6 required a simulation of the mechanism of reactions 1, 7, and 8. A potential influence of the chain process (reactions 9 and 10) was also examined. The simulation of the mechanism used tabulated equilibrium constants k_1/k_8 from ref 11 and results for k_7 from ref 9 (values for k_9 and k_{10} were only tentative; see ref 4). Modeled values of CF_2 yields Y ranged between ∼0.35 near 1750 K and 0.92 near 2100 K. One should note that even with reactant concentrations as low as 100 ppm (at temperatures near 1800 K), the effects of secondary bimolecular reactions could not be suppressed. Only at temperatures above 2000 K, the influence of secondary reactions decreased. Furthermore, at temperatures above 1600 K, no influence by reactions 9 and 10, which would have increased the CF_2 yield Y, was detected. The modeled kinetic profiles were characterized by a rapid initial increase of $[CF_2]$ with time, represented by eq 6, followed by only minor changes of the absorption levels attained on a much slower time scale. As the main part of the profile was given by eq 6, modeled kinetic profiles are not shown here. The experimental k and Y through $k_1 \approx Yk$ were converted to k_1; minor deviations from this simple analysis, whenever observed in the kinetic modeling, were accounted for, but always were smaller than the experimental scattering.

Table 1 summarizes representative rate constants k_1 as determined in the described way. Near 1800 K, $k_1/[Ar]$ is found to decrease by about a factor of 2, when $[Ar]$ increases from about 10^{-5} to 10^{-4} mol cm^{-3}. The reaction was thus studied close to (but not quite at) the low-pressure limit. The present results for $[Ar] \approx 10^{-5}$ mol cm^{-3} connect well with the results from ref 2 (for $[Kr]$ ranging up to 5.6×10^{-6} mol cm^{-3}). The dependence of k_1 on the bath gas concentrations $[M]$ is illustrated in Figure 3, where experimental data from the present work (with M = Ar) and from ref 2 (with M = Kr) are compared with modeled falloff curves; see below. Falloff curves are shown for 1800 and 2000 K; small "temperature mismatches" in the figure were accounted for by the modeled temperature dependences of k_1 at the given $[M]$; the temperature dependences of k_1 for two values of $[Ar]$ here are represented as

$$k_1 \propto \exp(-30\,200\ \text{K}/T)\text{s}^{-1} \qquad (11)$$

at $[Ar] \approx 10^{-5}$ mol cm^{-3} (for 1600−1800 K) and

Table 1. Representative Experimental Rate Constants for the Dissociation of CF_3 ($[CF_3]_{t=0}/[Ar]$ in ppm; T in K; $[Ar]$ in mol cm^{-3}; Rate Constants k_1 in s^{-1} Corrected for Secondary Reactions Contributing to k in eq 6, see Text; $Y = [CF_2]_{t=\infty}/[CF_3]_{t=0}$)

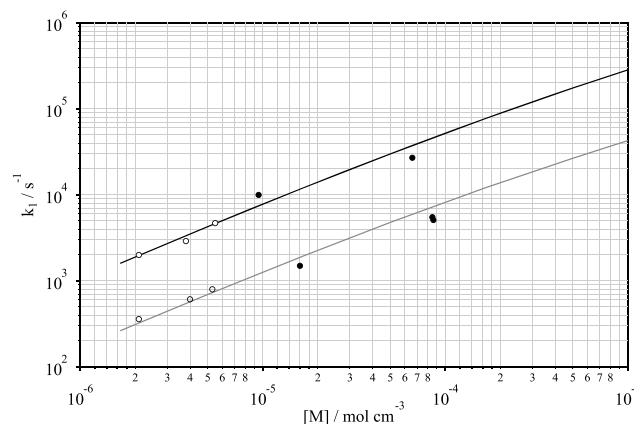| $[CF_3]_{t=0}/[Ar]$	T	$[Ar]$	k_1	Y
108	1690	$8.4 \cdot 10^{-5}$	$1.2 \cdot 10^3$	0.35
108	1742	$7.8 \cdot 10^{-5}$	$2.6 \cdot 10^3$	0.35
108	1826	$7.5 \cdot 10^{-5}$	$8.4 \cdot 10^3$	0.43
108	1885	$7.1 \cdot 10^{-5}$	$1.5 \cdot 10^4$	0.45
527	1870	$1.1 \cdot 10^{-5}$	$3.0 \cdot 10^3$	0.61
527	2024	$9.8 \cdot 10^{-6}$	$1.3 \cdot 10^4$	0.92
527	2106	$9.1 \cdot 10^{-6}$	$2.1 \cdot 10^4$	0.93
527	1743	$7.8 \cdot 10^{-5}$	$1.9 \cdot 10^3$	0.49
527	1778	$7.9 \cdot 10^{-5}$	$3.4 \cdot 10^3$	0.46
527	1943	$7.0 \cdot 10^{-5}$	$1.6 \cdot 10^4$	0.51
527	2038	$6.5 \cdot 10^{-5}$	$4.3 \cdot 10^4$	0.59
1054	1752	$7.9 \cdot 10^{-5}$	$7.5 \cdot 10^2$	0.54
1054	1859	$7.1 \cdot 10^{-5}$	$4.7 \cdot 10^3$	0.54
1054	1899	$7.1 \cdot 10^{-5}$	$1.2 \cdot 10^4$	0.50

Figure 3. Experimental pseudo-first-order rate constants k_1 of the dissociation of CF_3 in Ar (representative points from this work, filled circles) and in Kr (representative points from ref 2, open circle) converted to 1800 K (lower set of points) and 2000 K (upper set of points), in comparison with modeled falloff curves from this work (lines; see text).

$$k_1 \propto \exp(-29\,860\ \text{K}/T)\text{s}^{-1} \qquad (12)$$

at $[Ar] \approx 10^{-4}$ mol cm^{-3} (for 1800−2000 K). On the basis of these experimental results, complete falloff curves $k_1 ([M], T)$ were obtained with the help of the theoretical modeling described in the following section.

III. MODELING OF LIMITING RATE CONSTANTS

The present calculations of molecular parameters, as used for the modeling of rate constants, were performed at the G4// B3LYP/6-311+G(3df) ab initio level and, therefore, go beyond the less accurate G3//B3LYP/6-311G(d) calculations employed earlier.[3] Our procedure follows that described in detail in ref 4 and is not repeated here (details of the calculations are given in the Supporting Information). Morse parameters of the CF_2−F potential $V(r)$ were found to be $\beta_e = 2.42$ Å^{-1} (over the range $1.25 \leq r \leq 2.75$ Å) or $\beta_e = 2.90$ Å^{-1} (over the range $2.0 \leq r \leq 2.75$ Å). The frequencies of the two torsional transitional modes were found to decay exponentially with increasing bond length r (decay parameters of $\alpha = 1.71$ and

1.77 Å^{-1} were derived), such that the ratio α/β_c was found to be near 0.6. This ratio is only slightly above the "standard value" of 0.5[12] used in ref 3. Using molecular parameters for CF_3 and CF_2 as given in the Supporting Information, and the derived value of α/β_e, the limiting high-pressure rate constant was determined with the help of the classical trajectory version of the statistical adiabatic channel model (SACM/QT).[13] Values of

$$k_{1,\infty} = 1.6 \times 10^{16}(T/2000 \text{ K})^{-1.3}\exp(-43\,250 \text{ K}/T)\text{s}^{-1} \tag{13}$$

were obtained, approximately corresponding to

$$k_{1,\infty} \approx 4.6 \times 10^{15}\exp(-40\,760 \text{ K}/T)\text{s}^{-1} \tag{14}$$

The apparent activation energy of $k_{1,\infty}$ (339 kJ mol^{-1}) thus is not far from the threshold energy of reaction 1, i.e., 347.7 kJ mol^{-1}; see the Supporting Information. The rate constant of the reverse recombination of F with CF_2 followed as

$$k_{-1,\infty} = 1.0 \times 10^{14}(T/2000 \text{ K})^{0.09}\text{cm}^3\text{mol}^{-1}\text{s}^{-1} \tag{15}$$

Using an alternative quantum-chemical approach to the potential and variational transition state theory (VRC-TST), $k_{-1,\infty}$ (2000 K) in ref 2 was calculated to be 2.22×10^{13} cm^3 mol^{-1} s^{-1}. The difference of about a factor of 4.5 between the two approaches to $k_{1,\infty}$ has only a small influence on the experimentally observed part of the falloff curves. Nevertheless, it deserves an explanation, which is given in the Supporting Information.

Limiting low-pressure rate constants $k_{1,0}$ in the present work were obtained with the method of ref 7, fitting the average energy $\langle\Delta E\rangle$ transferred per collision with the help of the experimental results shown in Figure 3 and accounting for centrifugal barriers with the r-dependent rotational constants of CF_3 given in the Supporting Information. Values of $-\langle\Delta E\rangle/$hc ≈ 300 cm^{-1} (± 100 cm^{-1}) were fitted and, at least for the studied temperature range, were assumed to be independent of the temperature. Over the range 1500−2500 K, this led to rate constants

$$k_{1,0} = [\text{Ar}]2.5 \times 10^{18}(T/2000\text{K})^{-5.1}\exp(-42\,450 \text{ K}/T)$$
$$\text{cm}^3\text{mol}^{-1}\text{s}^{-1} \tag{16}$$

which can be approximated by

$$k_{1,0} = [\text{Ar}]2.5 \times 10^{16}\exp(-32\,835 \text{ K}/T)\text{cm}^3\text{mol}^{-1}\text{s}^{-1} \tag{17}$$

The master-equation approach of ref 2 over the range 1300−2500 K has given

$$k_{1,0} = [\text{Kr}]2.38 \times 10^{24}(T/298 \text{ K})^{-6.362}\exp(-45649 \text{ K}/T)$$
$$\text{cm}^3\text{mol}^{-1}\text{s}^{-1} \tag{18}$$

such that $k_{1,0}$ (2000 K) = [Kr] 1.6×10^9 cm^3 mol^{-1} s^{-1}, in comparison to $k_{1,0}$ (2000 K) = [Ar] 1.5×10^9 cm^3 mol^{-1} s^{-1} from the present modeling. A value of $-\langle\Delta E\rangle/$hc ≈ 420 cm^{-1} was estimated in ref 2, which corresponds to a collision efficiency β_c(2000 K) ≈ 0.16,[7] close to the value β_c(2000 K) ≈ 0.11 in the present calculation. The agreement between the two quite different approaches to $k_{1,0}$ thus appears quite satisfactory (one should note that the differences of the collision frequencies for M = Ar and Kr as well as the differences of $\langle\Delta E\rangle$ are only of minor importance).

IV. MODELED FALLOFF CURVES

Besides $k_{1,0}$ and $k_{1,\infty}$, center broadening factors F_{cent} enter the falloff expressions (reactions 3−5). As before,[4] we estimate their strong collision contribution $F_{\text{cent}}^{\text{sc}}$ by the method of ref 14, while a weak-collision contribution $F_{\text{cent}}^{\text{wc}} \approx 0.64$ in $F_{\text{cent}} \approx F_{\text{cent}}^{\text{sc}} F_{\text{cent}}^{\text{wc}}$ follows from ref 5. The resulting values here are $F_{\text{cent}} \approx 0.25$, 0.22, and 0.20 for T = 1500, 2000, and 2500 K, respectively. A value of 0.27 was derived in ref 2 (the difference, however, is of only small practical relevance, because the present experiments were conducted close to the low-pressure limit of the reaction. The difference is related to the different $k_{1,\infty}$ derived in the present work and in ref 2; see the Supporting Information).

In the following, two factors influencing the shape of the "broad" falloff curves of the present reaction[6] are inspected: (i) differences between the falloff expressions of eq 3 (from strong-collision, rigid-activated complex, Rice−Ramsperger−Kassel−Marcus (RRKM) theory[7]) and the falloff expressions of eqs 4 and 5 (from weak-collision master equations and loose-activated complex calculations[5]) and (ii) differences due to different $k_{1,0}$ and $k_{1,\infty}$.

Figure 4 compares falloff curves constructed with the simple falloff curves from eq 3 and the more elaborate expressions of
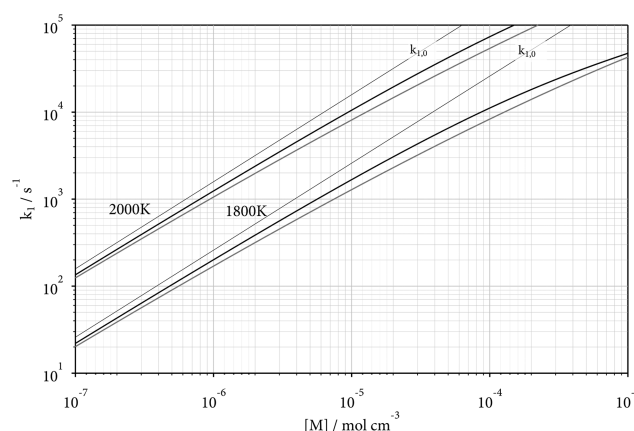

Figure 4. Comparison of modeled falloff representations by eq 3 (black line) and eqs 4 and 5 (gray line). The uppermost curves correspond to the low-pressure limiting $k_{1,0}$.

eqs 4 and 5 (using the same values of $k_{1,0}$, $k_{1,\infty}$, and F_{cent} as derived from the present modeling). The differences are clearly within the scatter of the experimental points shown in Figure 3 such that the simple eq 3 could be used as an alternative to eqs 4 and 5. Figure 5 provides a comparison of the present falloff curves with those from ref 2, employing markedly different values of $k_{1,\infty}$. Although the experimental scatter precludes any safe conclusions on $k_{1,\infty}$, the proximity of k_1 to $k_{1,0}$ is sufficient to permit a unique determination of $-\langle\Delta E\rangle/$hc (within an estimated accuracy of about ± 100 cm^{-1}).

V. CONCLUSIONS

It was shown that shock wave studies of the thermal dissociation 1 of CF_3 from ref 2 and from the present work are consistent with each other, provided that the influence of the secondary reactions (7 and 8) are taken into account. An influence of reactions 9 and 10, involving IF as an intermediate, could not be detected. The deduced rate constant k_1 was shown to correspond to conditions close to the limiting low-
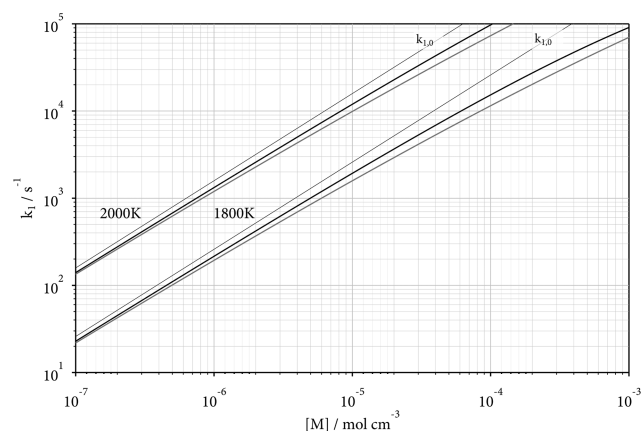
Figure 5. Comparison of modeled falloff curves from the present work (black line, eqs 4 and 5) and from the modeling of ref 2 (gray line) using different $k_{1,0}$ and $k_{1,\infty}$ (values given in the text). The uppermost curves correspond to the low-pressure limiting $k_{1,0}$.

pressure rate constant $k_{1,0}$ of the reaction. The influences of different falloff expressions (eq 3 vs eqs 4 and 5) and of different high-pressure rate constants $k_{1,\infty}$ on the evaluation of $k_{1,0}$ were investigated. Although the experimental scatter was apparently larger than the modeling differences of the falloff analysis, the present determination of a value of the total average energy $\langle \Delta E \rangle$ transferred per collision with the bath gas Ar, i.e., $-\langle \Delta E \rangle / hc \approx 300$ cm^{-1} (± 100) cm^{-1}, seems well founded. Although this value is somewhat higher than usually observed (see refs 4, 15), it does not appear unreasonable (the experiments from ref 2 for M = Kr would be evaluated with a very similar value of $\langle \Delta E \rangle$).

■ ASSOCIATED CONTENT

⒮ Supporting Information

The Supporting Information is available free of charge at https://pubs.acs.org/doi/10.1021/acs.jpca.9b10393.

Modeling of the Potential Energy Surface; Modeling of the Rate Constants; Molecular Parameters (PDF)

■ AUTHOR INFORMATION

Corresponding Author

J. Troe − *Institut für Physikalische Chemie, Universität Göttingen, D-37077 Göttingen, Germany; Max-Planck-Institut für Biophysikalische Chemie, D-37077 Göttingen, Germany;* ⓞ orcid.org/0000-0002-4347-0307; Email: juergen.troe@mpibpc.mpg.de

Authors

C. J. Cobos − *INIFTA, Facultad de Ciencias Exactas, Universidad Nacional de La Plata, CONICET, La Plata 1900, Argentina*

G. Knight − *Edwards Innovation Centre, Clevedon BS21 6TH, U.K.*

L. Sölter − *Institut für Physikalische Chemie, Universität Göttingen, D-37077 Göttingen, Germany*

E. Tellbach − *Institut für Physikalische Chemie, Universität Göttingen, D-37077 Göttingen, Germany*

Complete contact information is available at:
https://pubs.acs.org/10.1021/acs.jpca.9b10393

Notes

The authors declare no competing financial interest.

■ REFERENCES

(1) Modica, A. P.; Sillers, S. J. Experimental and Theoretical Kinetics of High-Temperature Fluorocarbon Chemistry. *J. Chem. Phys.* **1968**, *48*, 3283−3289.

(2) Srinivasan, N. K.; Su, M.-C.; Michael, J. V.; Jasper, A. W.; Klippenstein, S. J.; Harding, L. B. Thermal Decomposition of CF$_3$ and the Reaction of CF$_2$ + OH → CF$_2$O + H. *J. Phys. Chem. A* **2008**, *112*, 31−37.

(3) Cobos, C. J.; Croce, A. E.; Luther, K.; Troe, J. Shock Wave Study of the Thermal Decomposition of CF$_3$ and CF$_2$ Radicals. *J. Phys. Chem. A* **2010**, *114*, 4755−4761.

(4) Cobos, C. J.; Sölter, L.; Tellbach, E.; Troe, J. Falloff Curves and Mechanism of the Thermal Decomposition of CF$_3$I in Shock Waves. *Phys. Chem. Chem. Phys.* **2019**, *21*, 23893−23899.

(5) Troe, J.; Ushakov, V. G. Revisiting Falloff Curves of Thermal Unimolecular Reactions. *J. Chem. Phys.* **2011**, *135*, No. 054304.

(6) Troe, J.; Ushakov, V. G. Representation of "Broad" Falloff Curves for Dissociation and Recombination Reactions. *Z. Phys. Chem.* **2014**, *228*, 1−10.

(7) Troe, J. Predictive Possibilities of Unimolecular Rate Theory. *J. Phys. Chem. A.* **1979**, *83*, 114−126.

(8) Cobos, C. J.; Croce, A. E.; Luther, K.; Sölter, L.; Tellbach, E.; Troe, J. Experimental and Modeling Study of the Reaction C$_2$F$_4$ (+M) ↔ CF$_2$ + CF$_2$ (+M). *J. Phys. Chem. A* **2013**, *117*, 11420−11429.

(9) Knight, G.; Sölter, L.; Tellbach, E.; Troe, J. Shock Wave and Modeling Study of the Reaction CF$_4$ (+M) ↔ CF$_3$ + F (+M). *Phys. Chem. Chem. Phys.* **2016**, *18*, 17592−17596.

(10) Glänzer, K.; Maier, M.; Troe, J. Shock-Wave Study of the High-Temperature UV Absorption and the Recombination of CF$_3$ Radicals. *J. Phys. Chem. A.* **1980**, *84*, 1681−1686.

(11) Chase, M. W. NIST-JANAF Thermochemical Tables, Fourth Edition. *J. Phys. Chem. Ref. Data, Monogr.* **1998**, *9*, 1−1951.

(12) Cobos, C. J.; Troe, J. Theory of Thermal Unimolecular Reactions at High Pressures. II. Analysis of Experimental Results. *J. Chem. Phys.* **1985**, *83*, 1010−1015.

(13) Maergoiz, A. I.; Nikitin, E. E.; Troe, J.; Ushakov, V. G. Classical Trajectory and Statistical Adiabatic Channel Study of the Dynamics of Capture and Unimolecular Bond Fission. V. Valence Interactions between Linear Rotors. *J. Chem. Phys.* **1998**, *108*, 9987−9998.

(14) Troe, J. Theory of Thermal Unimolecular Reactions in the Falloff Range. I. Strong Collision Rate Constants. *Ber. Bunsenges. Phys. Chem.* **1983**, *87*, 161−169.

(15) Hippler, H.; Troe, J. Recent Direct Studies of Collisional Energy Transfer in Vibrationally Highly Excited Molecules in the Electronic Ground State. In *Gas Phase Bimolecular Processes*; Baggott, J. E.; Ashfold, M. N., Eds.; The Royal Society of Chemistry: London, 1988; pp 2019−2262.